Applied Surface Science 428 (2018) 1029–1035

Contents lists available at ScienceDirect

Applied Surface Science

journal homepage: www.elsevier.com/locate/apsusc

Full Length Article

# Native defects in silver orthophosphate and their effects on photocatalytic activity under visible light irradiation

Uyi Sulaeman[a,*], Dadan Hermawan[a], Roy Andreas[a], Ahmad Zuhairi Abdullah[b], Shu Yin[c]

[a] Department of Chemistry, Jenderal Soedirman University, Purwokerto, 53123, Indonesia
[b] School of Chemical Engineering, Universiti Sains Malaysia, 14300, Nibong Tebal, Penang, Malaysia
[c] Institute of Multidisciplinary Research for Advanced Materials, Tohoku University, Sendai, 980-8577, Japan

ARTICLE INFO

*Article history:*
Received 21 May 2017
Received in revised form 9 September 2017
Accepted 22 September 2017
Available online 28 September 2017

*Keywords:*
Defect
Co-precipitation
Photocatalyst
Silver orthophosphate
Silver vacancy

ABSTRACT

Native defects in silver orthophosphate could be generated by simple co-precipitation method under ethanol-aqueous solution using $AgNO_3$ and $Na_2HPO_4.12H_2O$. $AgNO_3$ ethanol-aqueous solution with the ethanol contents of 0%, 25%, 50%, 75%, 90% and 100% was reacted with $Na_2HPO_4$ aqueous solution. The produced catalysts were characterized using XRD, DRS, FE-SEM, BET specific surface area and XPS. The increase of ethanol content in the synthesis process decreased the Ag/P atomic ratio of $Ag_3PO_4$. The native defects of silver vacancy might be generated on the surface of $Ag_3PO_4$. The activity of $Ag_3PO_4$ for Rhodamine B degradation dramatically increased by 5.8 times higher compared to that of the pristine $Ag_3PO_4$. The defect states of Ag vacancies enhanced the separation of electron-hole pairs, leading to the improvement of photocatalytic activity.



## 1. Introduction

The improvement of $Ag_3PO_4$ activity for organic pollutant degradation has been mostly achieved by three strategies. The first is the design of particular morphology to generate high reactivity on the surface of $Ag_3PO_4$. These could create high surface energy [1] and the desired facet formation [2–4] to boost the activity of $Ag_3PO_4$ photocatalyst. The tetrahedron [1,4,5], tetrapod [3,6], ellipsoid [7] generally showed high activity under visible light irradiation. The high activity of tetrahedral $Ag_3PO_4$ is caused by {111} facets that contain only Ag atom [5]. The enriched $Ag^+$ cation in the {111} plane of $Ag_3PO_4$ could be partly reduced by photogenerated electron forming Ag nanolayers. These layers can facilitate the separation of photoexcited electron-hole pairs. The partially reduced $Ag^+$ site might produce a neighboring oxygen vacancy that increased the number of photocatalytic active sites. The tetrahedral morphology could also suppress the recombination of electron-hole pairs [4]. Saddle-like morphology of $Ag_3PO_4$ derived from tetrahedron also shows high photocatalytic activity due to an enriched $Ag^+$ on the surface [8]. The improved activity of tetrapod $Ag_3PO_4$ under visible light might be caused by the high activity of {110} facets [3,6] whereas the enhanced activity of the ellipsoid $Ag_3PO_4$ is caused by the clean surface of this particle and smaller band gap energy [7]. Morphology-dependent photocatalytic properties are very promising to provide the way forwards for highly active photocatalysts.

The second strategy of improving the $Ag_3PO_4$ activity is the design of heterostructure materials. These materials could prevent $Ag_3PO_4$ photocorrosion during the photocatalytic reaction and can enhance the separation of photogenerated electron and holes. The photocorrosion reaction always occurs in $Ag_3PO_4$ as its conduction band (CB) potential is more positive than the hydrogen potential which limits its potential applications in photocatalysis. Therefore many researchers have been dealing with this issue. The heterostructures of $Ag_3PO_4/TiO_2$ [9–12], $Ag_3PO_4/Cr\text{-}SrTiO_3$ [13], $Co_3O_4/Ag_3PO_4$ [14], $Ag_3PO_4$@$LaPO_4$ [15], $Ag_3PO_4/g\text{-}C_3N_4$ [16,17], $Ag_3PO_4/MoS_2$ [18] were successfully synthesized and improved activity and stability of photocatalyst. The responsible mechanism of these heterostructures could be a direct band-band transfer [19] and Z-scheme mechanism [17,20] between $Ag_3PO_4$ and its coupled semiconductor. A direct band-band transfer could be defined that the photogenerated electron in the CB of coupled semiconductor is transferred into the CB of $Ag_3PO_4$ and the photogenerated holes in the valence band (VB) of $Ag_3PO_4$ is transferred into the VB of coupled semiconductor [17]. In this mechanism, the hole of coupled semiconductor oxidizes the pollutants and the electron in the CB of $Ag_3PO_4$ produced reactive oxygen species during photocatalytic reaction. The Z-scheme mechanism could be defined that the photogenerated electrons in the CB of $Ag_3PO_4$ and photogenerated

* Corresponding author.
*E-mail address:* uyi_sulaeman@yahoo.com (U. Sulaeman).

https://doi.org/10.1016/j.apsusc.2017.09.188
0169-4332/

holes in the VB of coupled semiconductor combine directly [20] or through metallic particle contacted with both $Ag_3PO_4$ and coupled semiconductor [18,21,22]. This mechanism generates holes in the VB of $Ag_3PO_4$ and electron in the CB of coupled semiconductor [17].

The third strategy is the surface modification of $Ag_3PO_4$ by various electron or hole co-catalysts. This method can improve the photocatalytic performance via promoting the rapid transfer and separation of photogenerated charges. The $Ag_3PO_4$ surface could be modified by Co-Pi hole cocatalyst that improved the photocatalytic activity [23]. The simultaneous loading of Ag nanoparticles and Fe(III) co-catalyst could improve the photocatalytic activity of $Ag_3PO_4$ [24]. This Ag nanoparticles can generate the surface plasmon resonance and improves the bandgap visible-light absorption of $Ag_3PO_4$, resulting in the generation of more photogenerated charges. The surface of $Ag_3PO_4$ could also be modified by incorporating graphene to form $Ag_3PO_4$/graphene composite [25,26]. This modification improved the surface area, absorption of organic dyes and separation of photogenerated electron–hole pairs [25]. Incorporating graphene on the $Ag_3PO_4$ also improved the morphology in which the $Ag_3PO_4$ dispersed uniformly on the graphene sheets surface [26].

Recently, the presence of native defects in $Ag_3PO_4$ catalyst has tremendously attracted the attention of researchers [27]. $Ag_3PO_4$ with oxygen vacancy could be generated by calcination method [28]. During calcination, metallic Ag nanoparticle are formed and deposited on the surface of $Ag_3PO_4$. Oxygen vacancies have significant positive effect in improving the activity, whereas the metallic Ag nanoparticles have a very important effect in improving the stability. Chong et al. [29] reported that high temperature calcination of $Ag_3PO_4$ induced the oxygen vacancies. It is known that the enhanced photocatalytic activity of $Ag_3PO_4$ depends on crystallinity, oxygen vacancies and specific surface area. Unfortunately, the oxygen vacancy in $Ag_3PO_4$ has a relatively high formation energy compared to silver vacancy and silver interstitial because of the strong P-O bond that must be broken to remove an O atom [27]. Due to the strong P-O covalence, $PO_4^{3-}$ ions are difficult to form oxygen vacancies [30]. Therefore, generating the silver vacancy could be a promising approach to boost activity of $Ag_3PO_4$. Yan et al. [31] successfully synthesized $Ag_3PO_4$ with formation of metallic Ag and high Ag vacancies using silver acetate as the precursor followed by calcination. The improved photocatalytic activity of this material was due to the synergistic effect of Ag vacancies and metallic Ag, which contributed to the efficient separation of photogenerated charge carriers. Ma et al. [30] suggested that defect states of Ag vacancies could act as capture traps for photoexcited holes and enhanced the separation of photogenerated electron-hole pairs.

Here, native defects of Ag vacancy in $Ag_3PO_4$ were generated using co-precipitation method under ethanol-aqueous solution. $AgNO_3$ dissolved in ethanol-aqueous solution with the ethanol contents of 0%, 25%, 50%, 75%, 90% and 100% was reacted to $Na_2HPO_4$ aqueous solution. The enhanced composition of ethanol in the synthesis of $Ag_3PO_4$ decreased the Ag/P atomic ratio in $Ag_3PO_4$. These defects might facilitate the enhanced separation of photogenerated electron-hole which improved the photocatalytic activity.

## 2. Experimental

Silver vacancies of $Ag_3PO_4$ were prepared using co-precipitation method. Typically, 0.85 g of $AgNO_3$ was dissolved in 200 mL of ethanol-aqueous solution with ethanol contents of 0%, 25%, 50%, 75%, 90% and 100%. These samples were named as Et-0, Et-25, Et-50, Et-75, Et-90 and Et-100, respectively. $AgNO_3$ in ethanol-aqueous solution was slowly added (dropwise) by $Na_2HPO_4$ aqueous solution which was prepared by dissolving of 1.79 g of $Na_2HPO_4.12H_2O$ in 50 mL of water. The precipitates in this reaction were separated by 14,000 rpm centrifugation and washed with distilled water and acetone three times, and subsequently dried in a vacuum over night at 60 °C.

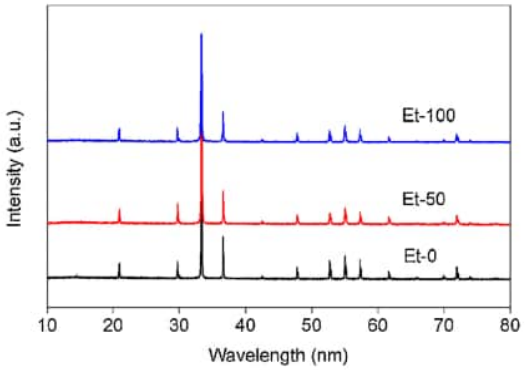


**Fig. 1.** XRD of $Ag_3PO_4$ synthesized using $Na_2HPO_4$ aqueous solution with $AgNO_3$ in ethanol (Et-100), 50% ethanol (Et-50) and without ethanol (Et-0).

The $Ag_3PO_4$ samples were characterized by X-ray diffraction (XRD, Bruker AXS D2 Phaser), while the diffuse reflection spectra were obtained using a UV-vis NIR spectrometer (JASCO V-670). The specific surface areas were determined by BET measurements (NOVA 4200e). The morphologies of the powders were observed by an FE-SEM (Hitachi, S-4800). The X-ray photoelectron spectra were obtained using an X-ray photoelectron spectrometer (XPS, Perkin Elmer PHI 5600).

The photocatalytic activities were evaluated based on the rate of Rhodamine B decomposition after dispersing 0.1 g of photocatalyst to 100 mL of 10 mg/L Rhodamine B aqueous solution. The mixture was stirred at room temperature for 2 min (under dark condition) and the 2.5 W of LED blue light (OptiLED, SP-E27BL, 2.5 W) was used for irradiation. Four ml of sample solution was withdrawn every 10 min and centrifugated at 14,000 rpm to separate the catalyst. The concentration of Rhodamine B was measured using a spectrophotometer (JASCO V-670). The highest photocatalytic activity was also evaluated using phenol (colorless pollutant) decomposition under blue light irradiation with the higher power (Duralux, E-27, 3 W). The phenol concentration was determined using 4-aminoantipyrine method.

The mechanisms of photocatalysis were investigated using the scavengers of radical and holes in photocatalytic reaction (10 mg/L RhB, 100 mL solution, 0.1 g catalyst) under blue light irradiation (Duralux, E-27, 3 W). The benzoquinone (BQ), isopropyl alcohol (IPA) and ammonium oxalate (AO) were added into solution as scavenger of superoxide ion ($O_2^{-}$•) radical, hydroxyl (•OH) radical and holes, respectively [32]. The scavenger dosage was 1 mmol/L and the concentration of Rhodamine B was measured using a spectrophotometer.

## 3. Results and discussion

A yellow-crystalline $Ag_3PO_4$ catalyst was successfully synthesized by a simple method of co-precipitation using $AgNO_3$ and $Na_2HPO_4.12H_2O$ as the starting materials. The $AgNO_3$ ethanol-aqueous solution with the ethanol concentrations of 0%, 25%, 50%, 75%, 90% and 100%, were successfully co-precipitated with $Na_2HPO_4$ aqueous solution. The XRD profiles shows that the structure of body-centered cubic (JCPDS no.06-0505) with the space group of P4-3n is observed in Et-0, Et-50 and Et-100 (Fig. 1). No impurities were detected in all samples, indicating that they are single phase. There is no difference of lattice constants that

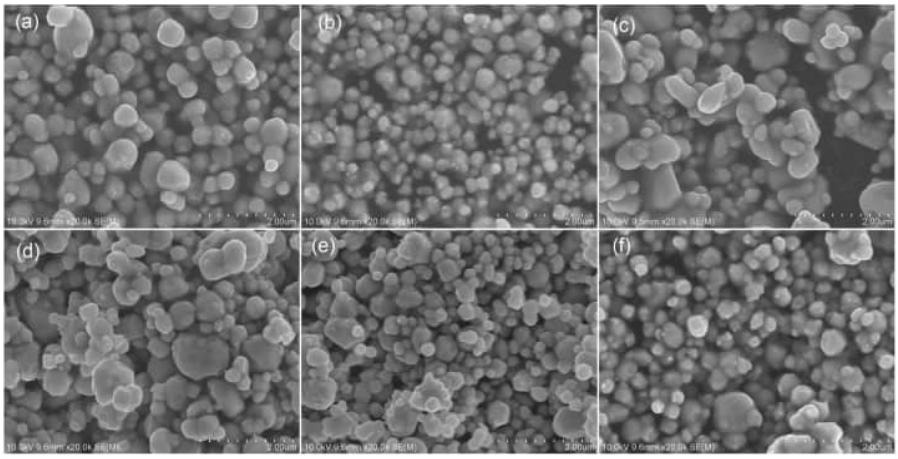


**Fig. 2.** SEM images of $Ag_3PO_4$ synthesized using $Na_2HPO_4$ aqueous solution and $AgNO_3$ in different compositions of ethanol-water: Et-0 (a), Et-25 (b), Et-50 (c), Et-75 (d), Et-90 (e) and Et-100 (f).

**Table 1**
Specific surface area, band gap energy and rate constant of $Ag_3PO_4$ synthesized under different compositions of ethanol-water solution.

| Sample | S.S.A. ($m^2$/g) | Band gap energy (eV) | $K_{app}$ ($min^{-1}$) |
|---|---|---|---|
| Et-0 | 7.18 | 2.40 | 0.018 |
| Et-25 | 8.34 | 2.37 | 0.051 |
| Et-50 | 4.46 | 2.38 | 0.105 |
| Et-75 | 7.67 | 2.37 | 0.095 |
| Et-90 | 4.11 | 2.38 | 0.106 |
| Et-100 | 9.12 | 2.40 | 0.069 |

could be observed in the samples. The lattice constants of 6.0148Å, 6.0149Å, 6.0149 Å could be calculated in the Et-0, Et-50 and Et-100, respectively. All structures were similar to those reported previously using $H_3PO_4$ in ethanol solution as the source of phosphate ion [8]. However, in the recent synthesis, there was no tetrahedral morphology that could be formed. The sphere and irregular shapes were clearly observed in all samples with the particle sizes of 200–600 nm as shown in Fig. 2(a–f). Specific surface areas of 4.46–9.12 $m^2$/g could be obtained and there is no significant difference of the specific surface area (Table 1). These indicated that the high photocatalytic activity did not depend on specific surface area or morphologies. Some other effects such as defect properties should be investigated to understand the reason of enhanced photocatalytic activity.

Fig. 3 shows the absorption spectra of Et-0, Et-50 and Et-100. It is clearly noted that the broad absorption above 500 nm increased in Et-50 and Et-100. It indicates that the ethanol treatment in the solution affects the optical properties of $Ag_3PO_4$. The absorption of $Ag_3PO_4$ is very important to act as visible-responsive photocatalyst. Some researchers found that the broad absorption in visible region might come from the defect sites of crystals as found in $TiO_2$ [33] and $SrTiO_3$ [34]. In this experiment, the broad absorption in visible region could be found in $Ag_3PO_4$ prepared by ethanol-water solution. The band gap energy ($E_g$) of photocatalyst can be calculated using the following equation [35]: $\alpha h\nu = A(h\nu - E_g)^{n/2}$ where $\alpha$, h and $\nu$ are the absorption coefficient, Planck constant, light frequency, respectively, while A is a constant and the value of n depends on whether the transition is direct (n = 1) or indirect (n = 4). The calculated band gap energies of all samples are similar as shown in Table 1. Therefore, the phenomenon of broad absorption in visible region might play a key role in photocatalytic activity under visible light irradiation. This phenomenon is also discussed in detail in the section of XPS analysis.

Fig. 4 shows the photocatalytic decomposition of Rhodamine B (RhB) under blue light irradiation (LED 2.5 W). The apparent pseudo-first-order kinetics equation of $\ln(C_0/C) = K_{app}t$ was used to evaluate the rate of photocatalytic reaction, where $K_{app}$ is the apparent pseudo-first-order rate constant ($min^{-1}$), C and $C_0$ are the RhB concentration at time t and zero, respectively [36,37]. The calculated values of $K_{app}$ are summarized in Table 1. Based on these results, all samples synthesized with the ethanol-water solution showed higher activity. The highest activities were observed in Et-50 and Et-90. The photocatalytic activity could be improved to about 5.8 times higher than that of the Et-0. This activity was higher than the previous result of saddle-like $Ag_3PO_4$ which was about 3 times higher compared to its control [8]. This observation suggests that the activity of $Ag_3PO_4$ was significantly affected by the type of starting materials and composition of solution. In this experiment, the photocatalytic activities were significantly influenced by the properties of $Ag_3PO_4$ which was formed by varying the ethanol content in the $Ag^+$ solution and $Na_2HPO_4$ aqueous solution. The different properties might be attributed to different co-precipitation condition due to different polarity of the mixed

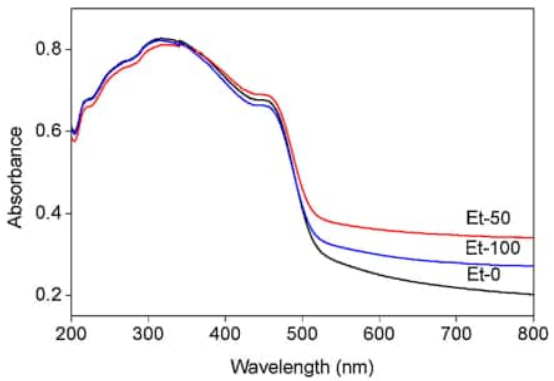


**Fig. 3.** DRS of $Ag_3PO_4$ synthesized using $Na_2HPO_4$ aqueous solution and $AgNO_3$ in ethanol (Et-100), 50% ethanol in ethanol-water solution (Et-50) and without ethanol (Et-0).

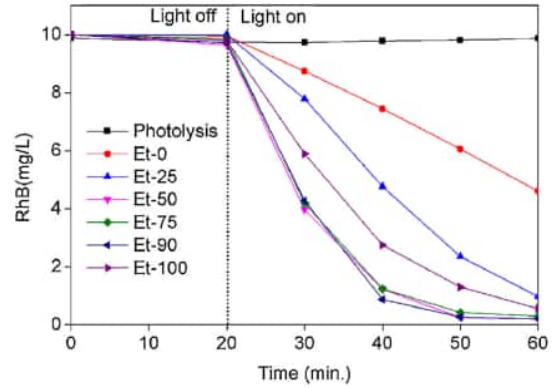


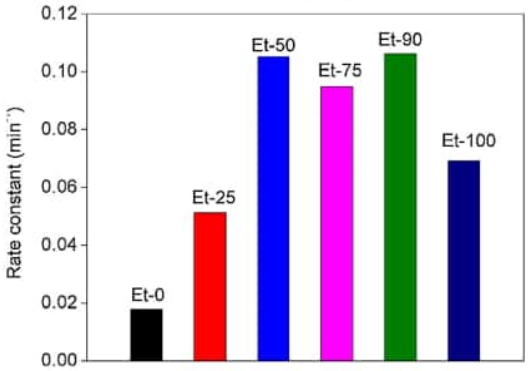


**Fig. 4.** Photocatalytic activities of $Ag_3PO_4$ synthesized using $Na_2HPO_4$ aqueous solution and $AgNO_3$ in different compositions of ethanol-water: Et-0, Et-25, Et-50, Et-75, Et-90 and Et-100 under blue light irradiation (LED 2.5W).

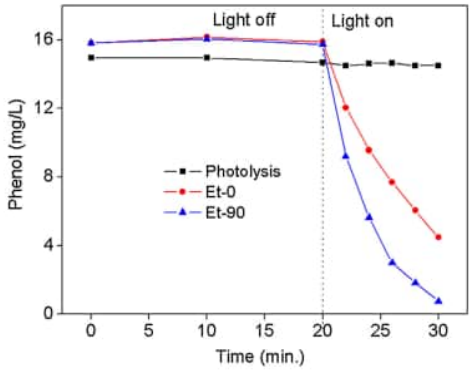


**Fig. 5.** Photocatalytic phenol degradation using Et-0 and Et-90 under blue light irradiation (LED 3 W).

solutions. The mixed solution would affect the migration of ions in the solution and influence the co-precipitation, which causes the defect sites trapped in the bulk or the surface of $Ag_3PO_4$ particles. These native defects might be a silver vacancy state which facilitates the enhanced separation of photogenerated electron-hole.

To ensure the effect of defect sites, the photocatalytic activity was also applied to decompose the phenol compound (the colorless pollutant) under blue light irradiation with the higher power of LED lamp (3 W) (Fig. 5). The highest photocatalytic activity of Et-90 was evaluated by phenol decomposition and the result was compared

**Table 2**
Peak energy and FWHM of Ag4d, P2p and O1s from the XPS analysis.

| Sample | Element | Peak energy (eV) | FWHM (eV) |
|---|---|---|---|
| Et-0 | Ag4d | 4.99 | 2.90 |
| | P2p | 132.61 | 2.13 |
| | O1s(O1) | 530.52 | 1.62 |
| | O1s(O2) | 532.34 | 2.06 |
| Et-50 | Ag4d | 5.00 | 2.80 |
| | P2p | 132.86 | 2.23 |
| | O1s(O1) | 530.60 | 1.55 |
| | O1s(O2) | 532.46 | 2.03 |
| Et-100 | Ag4d | 4.81 | 2.77 |
| | P2p | 132.74 | 2.21 |
| | O1s(O1) | 530.52 | 1.53 |
| | O1s(O2) | 532.40 | 1.93 |

to Et-0. The rate constant of 0.286 $min^{-1}$ could be observed in Et-90 which is significantly higher than that of Et-0 (0.124 $min^{-1}$) indicating that the photocatalyst is not only active for color pollutant degradation but also for colorless pollutant.

The XPS investigation was carried out to understand the properties of Et-0, Et-50 and Et-100 (Fig. 6 (a,b)). The peaks at 4.99 eV, 5.00 and 4.81 eV could be attributed to Ag4d of Et-0, Et-50 and Et-100 respectively. The peak energy of Ag4d of Et-50 is similar to that of Et-0, whereas the peak of Et-100 shifts to the lower binding energy by 0.18 eV. The peak energies of 132.61, 132.86 and 132.74 eV attributed to $P^{5+}$ of $Ag_3PO_4$ are observed in Et-0, Et-50 and Et-100 respectively [38]. The peak energy of P2p is shifted by 0.25 eV to a higher energy for Et-50. Interestingly, the full width at half maximum (FWHM) of Ag4d decreases with the addition of ethanol whereas the FWHM of P2p increases with the addition of ethanol in synthesis of $Ag_3PO_4$. The decreased FWHM of Ag4d and increased FWHM of P2p might be attributed to the silver vacancy formation. The details of peak energy and FWHM of Et-0, Et-50 and Et-100 are summarized in Table 2.

The changes of these states could be explained by theoretical aspect of Ag vacancy as described by Reunchan and Umezawa [27]. The Ag vacancy ($V_{Ag}$) formation did not require much energy because the Ag—O bonds are weak and can be easily broken, whereas oxygen vacancy ($V_o$) needs high energy due to the strong bonding of P-O. With the absence of Ag atom, the partially occupied states in the band gap could be created. These were mostly derived from the d orbitals of a neighboring Ag atom. These states could accept an additional electron to form a single acceptor of Ag vacancy ($V_{Ag}$). As the $V_{Ag}$ is an acceptor, the negative charge state ($V^-_{Ag}$) is more easily formed when Fermi energy ($\varepsilon_F$) increases.

The decreased FWHM of Ag4d might be the consequence of shorter distance of the two Ag atoms due to the $V_{Ag}$. Theoretically [27], the distance of the two Ag atoms across the $V_{Ag}$ is shorter than the equilibrium distance of the corresponding two Ag atoms in the perfect crystal. The strong attractive interaction between the $V_{Ag}$ and the neighboring Ag atoms might lead to a high $V_{Ag}$ mobility. The low energy migration barrier of $V^-_{Ag}$ suggests that the $V^-_{Ag}$ probably migrates along the path which involves the displacement of the nearest-neighboring Ag atom. Therefore, the silver vacancies could not be the isolated defects. They could bind with other defects or impurities, diffuse out of the bulk region, or possibly migrate and become trapped on the surface of the $Ag_3PO_4$ particles.

The atomic ratio of Ag/P significantly decreases by increasing the ethanol content indicating that the silver vacancy could be easily created (Table 3). Theoretically [27], the main native defects of $Ag_3PO_4$ could be a silver vacancy ($V_{Ag}$), oxygen vacancy ($V_O$), silver interstitial ($Ag_i$), oxygen interstitial ($O_i$), and interstitial hydrogen ($H_i$). Among these defects, silver vacancy is easier created in $Ag_3PO_4$ due to low energy of formation. Previous work, the defects could be designed by non-stoichiometric synthesis of photocatalyst [39]. Here, the different polarity of the mixed solutions might also affect

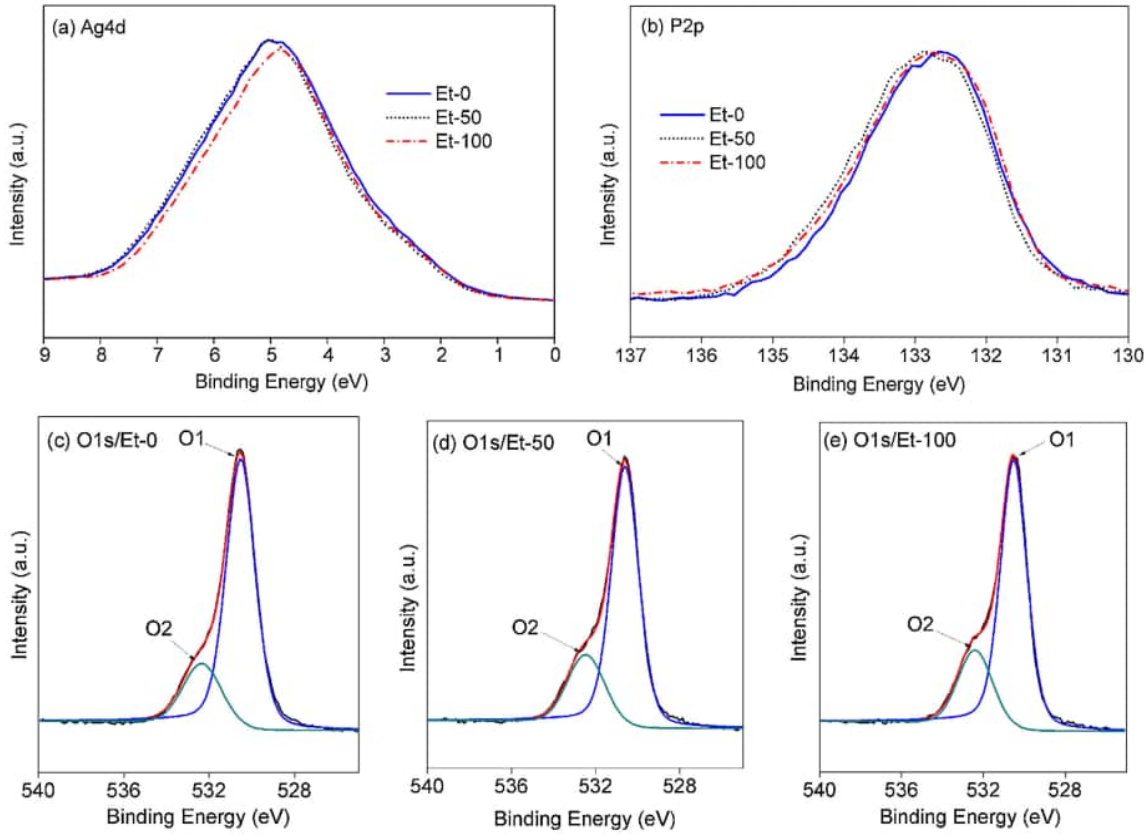


**Fig. 6.** XPS profiles of $Ag_3PO_4$ for Et-0, Et-50 and Et-100: the Ag4d (a), P2p (b) and O1s with the deconvolution of Et-0 (c), Et-50 (d) and Et-100 (e).

**Table 3**
Atomic ratios of Ag/P and O/Ag in the samples of Et-0, Et-50 and Et-100.

| Sample | Atomic Ratio | |
|---|---|---|
| | Ag/P | O/Ag |
| Et-0 | 2.66 | 1.39 |
| Et-50 | 2.57 | 1.52 |
| Et-100 | 2.41 | 1.55 |

the atomic ratio of $Ag_3PO_4$. The decrease of Ag/P atomic ratio, the decrement of the Ag4d FWHM and increment of P2p FWHM of $Ag_3PO_4$ indicate that the silver vacancies were formed.

The atomic ratio of O/Ag in $Ag_3PO_4$ increases by elevating the ethanol content of mixed solution (Table 3). To understand the type of oxygen in $Ag_3PO_4$, the deconvolution of O1s peak should be created using the Lorentziane Gaussian fitting. There are two types of peaks (O1 and O2) were observed as shown in Fig. 6 (c–e). The O1 peak at 530.52 eV is related to O—Ag bonding whereas the O2 peak (shoulder peak) at 532.34 eV could be assigned to hydroxyl groups [29,40]. The O2 peak of hydroxyl groups might be attributed to the interaction of $H_2O$ on the $Ag_3PO_4$ surface. From the deconvolution, the O2/O1 area ratio of 0.25, 0.29 and 0.32 could be calculated in Et-0, Et-50 and Et-100 respectively, indicating that the samples with the ethanol treatment might have higher amount of hydroxyl groups on the surface. The Ag vacancy created in Et-50 and Et-100 might enhance the interaction of $PO_4^{3-}$ and $H_2O$ in the surface. These can facilitate the formation of hydroxyl radical under visible light irradiation. The inductive effect of $PO_4^{3-}$ could also enhance the electron and holes separation, which plays an important role in photocatalysis [41].

The mechanisms of photocatalytic were investigated by adding the scavengers of radicals and holes to photocatalytic reaction [32]. The benzoquinone (BQ), isopropyl alcohol (IPA) and ammonium oxalate (AO) were added into the reaction solution as scavenger of superoxide ion ($O_2^{-\bullet}$) radicals, hydroxyl ($^{\bullet}OH$) radicals and holes, respectively. The effect of these scavengers to photocatalytic reaction can be seen in Fig. 7. The BQ addition could significantly suppress the photocatalytic activity in both Et-0 and Et-50, indicating that their mechanisms involved the superoxide ion radicals. The addition of IPA suppress the photocatalytic activity of Et-50, suggesting that the mechanism involved the hydroxyl radicals which might be generated by the defect sites of $Ag_3PO_4$ surface, whereas the photocatalytic activity in Et-0 could not be significantly suppressed by adding IPA, indicating that the mechanism might not involve the hydroxyl radical. Generating hydroxyl radical in Et-50 correspond with the XPS analysis that showing the higher ratio of O2/O1 due to higher amount of hydroxyl group adsorption in the surface of $Ag_3PO_4$. The $PO_4^{3-}$ on the surface of $Ag_3PO_4$ might play as the strong bonding ability with $H_2O$ that can promote hydroxyl radical formation. The addition of AO to Et-0 and Et-50 suppressed their photocatalytic activity, indicating both of them involved the holes mechanism. The higher suppression was found in Et-50, suggesting that the holes were highly involved in the mechanism of photocatalytic. The Ag vacancy sites in the band gap of $Ag_3PO_4$ will act as capture traps for photoexcited holes, which subsequently enhances the separation of electron-hole pairs resulting in improvement in

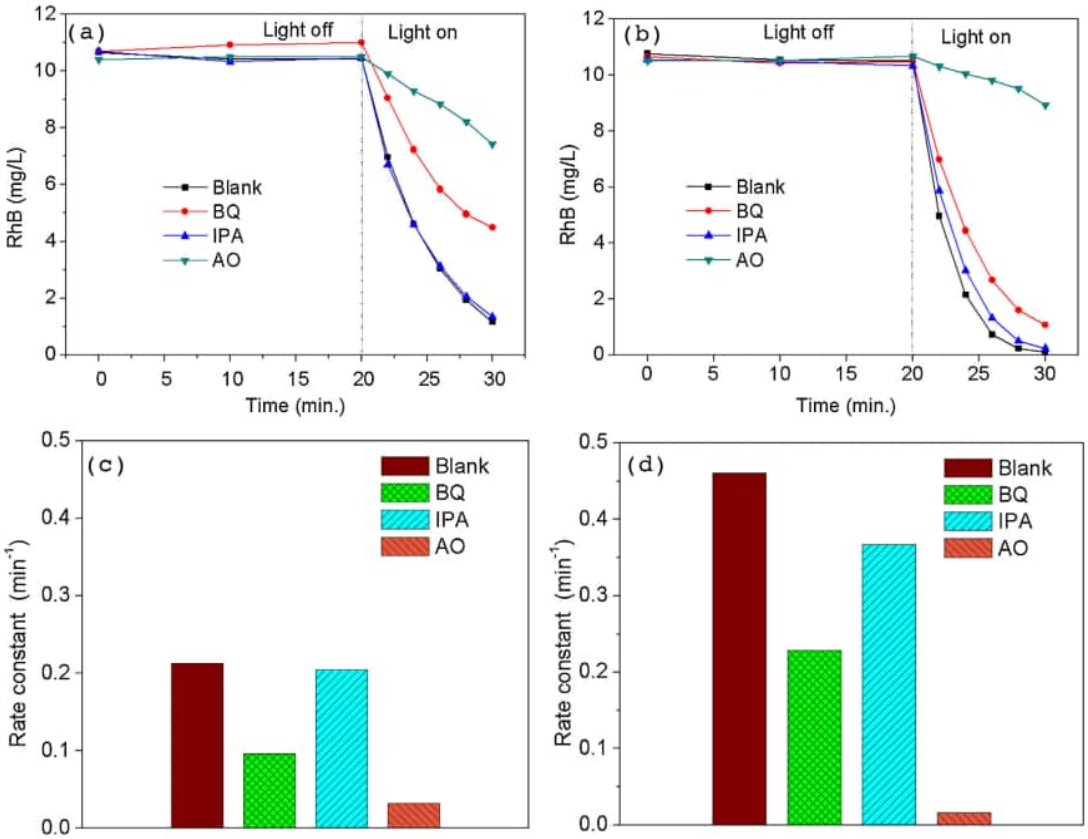


**Fig. 7.** The effect of benzoquinone (BQ), isopropyl alcohol (IPA) and ammonium oxalate (AO) on the photocatalytic reaction in Et-0 (a), Et-50(b) and the rate constant in Et-0 (c), Et-50(d).

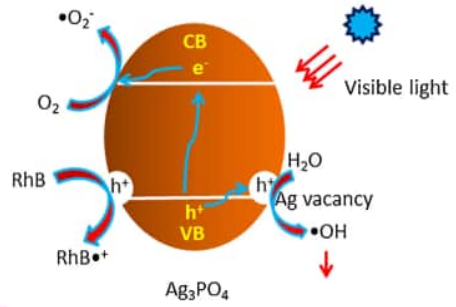


**Fig. 8.** The proposed mechanism of photocatalytic reaction in the surface of defect $Ag_3PO_4$.

photocatalytic activity. The holes accumulated at the valence band of $Ag_3PO_4$ might directly oxidize RhB to produce $RhB^{\bullet+}$ radicals, and the exited electron at the conduction band of $Ag_3PO_4$ transfer to adsorbed oxygen to form $^{\bullet}O_2^-$. The mechanism of photocatalytic reaction was proposed in Fig. 8

## 4. Conclusions

The $Ag_3PO_4$ photocatalyst with native defects were successfully synthesized through co-precipitation method using $AgNO_3$ ethanol-aqueous solution and $Na_2HPO_4$ aqueous solution. Elevated ethanol concentration evidently decreased the Ag/P atomic ratio of $Ag_3PO_4$. The broad absorption in visible region of DRS, the decrement of the 3d4d FWHM and increment of P2p FWHM might be caused by a silver vacancy formation on the surface of $Ag_3PO_4$. The photocatalytic activity of $Ag_3PO_4$ with silver vacancy increased to about 5.8 times higher than that of the pristine $Ag_3PO_4$. The defect states of Ag vacancies could act as capture traps for photoexited holes, which subsequently enhances the separation of electron-hole pairs, leading to the enhancement of photocatalytic activity.

## Acknowledgments

This research was financially supported by Directorate of Research and Community Services, Directorate General of Development and Research Enhancement, Ministry of Research, Technology and Higher Education of the Republic of Indonesia in the Scheme of Competency Grant, Contract Number: 068/SP2H/LT/DRPM/IV/2017.

## References

[1] D.J. Martin, N. Umezawa, X. Chen, J. Ye, J. Tang, Energy Environ. Sci. 6 (2013) 3380–3386.
[2] Y. Bi, S. Ouyang, N. Umezawa, J. Cao, J. Ye, J. Am. Chem. Soc. 133 (2011) 6490–6492.
[3] H. Wang, L. He, L. Wang, P. Hu, L. Guo, X. Han, J. Li, CrystEngComm 14 (2012) 8342–8344.

[4] B. Zheng, X. Wang, C. Liu, K. Tan, Z. Xie, L. Zheng, J. Mater. Chem. A 1 (2013) 12635–12640.
[5] H. Hu, Z. Jiao, H. Yu, G. Lu, J. Ye, Y. Bi, J. Mater. Chem. A 1 (2013) 2387–2390.
[6] J. Wang, F. Teng, M. Chen, J. Xu, Y. Song, X. Zhou, CrystEngComm 15 (2013) 39–42.
[7] P.W. Menezes, A. Indra, M. Schwarze, F. Schuster, M. Driess, ChemPlusChem 81 (2016) 1–8.
[8] U. Sulaeman, F. Febiyanto, S. Yin, T. Sato, Catal. Commun. 85 (2016) 22–25.
[9] L. Yang, W. Duan, H. Jiang, S. Luo, Y. Luo, Mater. Res. Bull. 70 (2015) 129–136.
[10] P.S. Saud, B. Pant, A.P. Twari, Z.K. Ghouri, M. Park, H.-Y. Kim, J. Colloid Interface Sci. 465 (2016) 225–232.
[11] C. Liu, X. Zhang, Q. Zhang, G. Meng, H. Zhao, J. Wu, Z. Liu, J. Porous Mater. 24 (2017) 179–187.
[12] B. Liu, Y. Xue, J. Zhang, B. Han, J. Zhang, X. Suo, L. Mu, H. Shi, Environ. Sci. Nano 4 (2017) 255–264.
[13] J. Guo, S. Ouyang, P. Li, Y. Zhang, T. Kako, J. Ye, Appl. Catal. B Environ. 134–135 (2013) 286–292.
[14] C. Tang, E. Liu, J. Wan, X. Hu, J. Fan, Appl. Catal. B Environ. 181 (2016) 707–715.
[15] F. Li, Z. Li, Y. Cai, M. Zhang, Y. Shen, X. Wang, M. Wu, Y. Li, C. Chen, X. He, Mater. Lett. 188 (2017) 343–346.
[16] P. He, L. Song, S. Zhang, X. Wu, Q. Wei, Mater. Res. Bull. 51 (2014) 432–437.
[17] L. Zhou, W. Zhang, L. Chen, H. Deng, J. Colloid Interface Sci. 487 (2017) 410–417.
[18] C. Zhua, L. Zhang, B. Jiang, J. Zheng, P. Hu, S. Li, M. Wu, W. Wu, Appl. Surf. Sci. 377 (2016) 99–108.
[19] N.N. Wang, Y. Zhou, C.H. Chen, L.Y. Cheng, H.M. Ding, Catal. Commun. 73 (2016) 74–79.
[20] S. Meng, X. Ning, T. Zhang, S. Chen, X. Fu, Phys. Chem. Chem. Phys. 17 (2015) 11577–11585.
[21] Y.F. Wang, J.X. Liu, Y.W. Wang, C.M. Fan, G.Y. Ding, Mater. Sci. Semicond. Process. 25 (2014) 330–336.
[22] J.X. Liu, Y.F. Wang, Y.W. Wang, C.M. Fan, Acta Phys.–Chim. Sin. 30 (2014) 729–737.
[23] P. Wang, S. Xu, Y. Xia, X. Wang, H. Yu, J. Yub, Phys. Chem. Chem. Phys. 19 (2017) 10309–10316.
[24] H. Yu, G. Cao, F. Chen, X. Wang, J. Yu, M. Lei, Appl. Catal. B Environ. 160–161 (2014) 658–665.
[25] X. Yang, H. Cui, Y. Li, J. Qin, R. Zhang, H. Tang, ACS Catal. 3 (2013) 363–369.
[26] L. Xu, Y. Wang, J. Liu, S. Han, Z. Pan, L. Gan, J. Photochem. Photobiol. A Chem. 340 (2017) 70–79.
[27] P. Reunchan, N. Umezawa, Phys. Rev. B 87 (2013) 245205.
[28] P. Dong, G. Hou, C. Liu, X. Zhang, H. Tian, F. Xu, X. Xi, R. Shao, Materials 9 (2016) 968.
[29] R. Chong, X. Cheng, B. Wang, D. Li, Z. Chang, L. Zhang, Int. J. Hydrogen Energy 41 (2016) 2575–2582.
[30] X. Ma, B. Lu, D. Li, R. Shi, C. Pan, Y. Zhu, J. Phys. Chem. C 115 (2011) 4680–4687.
[31] T. Yan, W. Guan, J. Tian, P. Wang, W. Li, J. You, B. Huang, J. Alloy Compd. 680 (2016) 436–445.
[32] W. Liu, M. Wang, C. Xu, S. Chen, X. Fu, Mater. Res. Bull. 48 (2013) 106–113.
[33] I. Nakamura, N. Negishi, S. Kutsuna, T. Ihara, S. Sugihara, K. Takeuchi, J. Mol. Catal. A: Chem. 161 (2000) 205–212.
[34] H. Tan, Z. Zhao, W. Zhu, E.N. Coker, B. Li, M. Zheng, W. Yu, H. Fan, Z. Sun, ACS Appl. Mater. Interfaces 6 (2014) 19184–19190.
[35] M.A. Butler, J. Appl. Phys. 48 (1977) 1914–1920.
[36] Y. Li, X. Li, J. Li, J. Yin, Water Res. 40 (2006) 1119–1126.
[37] U. Sulaeman, X. Wu, B. Liu, S. Yin, T. Sato, Appl. Surf. Sci. 356 (2015) 226–231.
[38] R. Zheng, L. Lin, J. Xie, Y. Zhu, Y. Xie, J. Phys. Chem. C 112 (2008) 15502–15509.
[39] U. Sulaeman, S. Yin, T. Sato, Appl. Phys. Lett. 97 (2010) 103102.
[40] W. Teng, X. Li, Q. Zhao, G. Chen, J. Mater. Chem. A 1 (2013) 9060–9068.
[41] C. Pan, Y. Zhu, Environ. Sci. Technol. 44 (2010) 5570–5574.

# jurnal 2

ORIGINALITY REPORT

| 23% | 7% | 22% | 2% |
|---|---|---|---|
| SIMILARITY INDEX | INTERNET SOURCES | PUBLICATIONS | STUDENT PAPERS |

PRIMARY SOURCES

| | | |
|---|---|---|
| 1 | Pakpoom Reunchan, Naoto Umezawa. " Native defects and hydrogen impurities in Ag PO ", Physical Review B, 2013<br>Publication | 3% |
| 2 | daneshyari.com<br>Internet Source | 3% |
| 3 | Ruidi Liu, Hui Li, Libing Duan, Hao Shen, Qian Zhang, Xiaoru Zhao. "The synergistic effect of graphene oxide and silver vacancy in Ag 3 PO 4 -based photocatalysts for rhodamine B degradation under visible light", Applied Surface Science, 2018<br>Publication | 2% |
| 4 | Uyi Sulaeman, Febiyanto Febiyanto, Shu Yin, Tsugio Sato. "The highly active saddle-like Ag3PO4 photocatalyst under visible light irradiation", Catalysis Communications, 2016<br>Publication | 2% |
| 5 | Xinguo Ma, Bin Lu, Di Li, Rui Shi, Chenshi Pan, Yongfa Zhu. "Origin of Photocatalytic Activation of Silver Orthophosphate from | 2% |

First-Principles", The Journal of Physical Chemistry C, 2011
Publication

| | | |
|---|---|---|
| 6 | Mohammad Afif, Uyi Sáulaeman, Anung Riapanitra, Roy Andreas, Shu Yin. "Use of Mn Doping to Suppress Defect Sites in Ag3PO4: Applications in Photocatalysis", Applied Surface Science, 2018<br>Publication | 2% |
| 7 | zombiedoc.com<br>Internet Source | 1% |
| 8 | Li Zhou, Wei Zhang, Ling Chen, Huiping Deng. "Z-scheme mechanism of photogenerated carriers for hybrid photocatalyst Ag 3 PO 4 /g-C 3 N 4 in degradation of sulfamethoxazole", Journal of Colloid and Interface Science, 2017<br>Publication | 1% |
| 9 | Uyi Sulaeman, Syarifah Fauziyyah Ramadhanti, Hartiwi Diastuti, Ponco Iswanto, Isnaeni Isnaeni, Shu Yin. "The enhanced photo-stability of defective Ag3PO4 tetrahedron prepared using tripolyphosphate", Arabian Journal of Chemistry, 2022<br>Publication | 1% |
| 10 | Julia Zwara, Ewelina Grabowska, Tomasz Klimczuk, Wojciech Lisowski, Adriana Zaleska-Medynska. "Shape-dependent enhanced | 1% |

photocatalytic effect under visible light of Ag3PO4 particles", Journal of Photochemistry and Photobiology A: Chemistry, 2018
Publication

11 Roy Andreas, Aldes Lesbani, Faqihudin Akhmad Yusuf. "The character istics (compositions, morphological, and structure) of nanocomposites polyaniline (PANI)/ZnO", IOP Conference Series: Materials Science and Engineering, 2019 — 1 %
Publication

12 Yu, Huogen, Guoqiang Cao, Feng Chen, Xuefei Wang, Jiaguo Yu, and Ming Lei. "Enhanced photocatalytic performance of Ag3PO4 by simutaneous loading of Ag nanoparticles and Fe(III) cocatalyst", Applied Catalysis B Environmental, 2014. — 1 %
Publication

13 Fang, Shun, Kangle Lv, Qin Li, Hengpeng Ye, Dongyun Du, and Mei Li. "Effect of acid on the photocatalytic degradation of rhodamine B over g-C3N4", Applied Surface Science, 2015. — 1 %
Publication

14 Uyi Sulaeman, Yusvirza Khairullah Gandasasmita, Hartiwi Diastuti, Ponco Iswanto, Isnaeni, Ardiansyah Taufik, Shu Yin. "Surface modification of Ag3PO4 using the alginate for highly active photocatalyst under — 1 %

visible light irradiation", Surfaces and Interfaces, 2021
Publication

15 Chong, Ruifeng, Xiaoxue Cheng, Baoyun Wang, Deliang Li, Zhixian Chang, and Ling Zhang. "Enhanced photocatalytic activity of Ag3PO4 for oxygen evolution and Methylene blue degeneration: Effect of calcination temperature", International Journal of Hydrogen Energy, 2016.
Publication

1 %

16 Uyi Sulaeman, Richo Dwi Permadi, Dian Riana Ningsih, Hartiwi Diastuti, Anung Riapanitra, Shu Yin. "The surface modification of Ag3PO4 using anionic platinum complexes for enhanced visible-light photocatalytic activity", Materials Letters, 2020
Publication

1 %

17 Sugang Meng, Xiaofeng Ning, Tao Zhang, Shi-Fu Chen, Xianliang Fu. " What is the transfer mechanism of photogenerated carriers for the nanocomposite photocatalyst Ag PO /g-C N , band–band transfer or a direct Z-scheme? ", Physical Chemistry Chemical Physics, 2015
Publication

1 %

Exclude quotes On

Exclude matches < 1%

Exclude bibliography On